ISSN 1063-7834, Physics of the Solid State, 2007, Vol. 49, No. 9, pp. 1749–1758. © Pleiades Publishing, Ltd., 2007.
Original Russian Text © V.I. Zinenko, M.S. Pavlovskiĭ, 2007, published in Fizika Tverdogo Tela, 2007, Vol. 49, No. 9, pp. 1668–1675.

LATTICE DYNAMICS AND PHASE TRANSITIONS

Lattice Dynamics and the Phase Transition from the Cubic Phase to the Tetragonal Phase in the $LaMnO_3$ Crystal within the Polarizable-Ion Model

V. I. Zinenko and M. S. Pavlovskiĭ

Kirensky Institute of Physics, Siberian Division, Russian Academy of Sciences, Krasnoyarsk, 660036 Russia
e-mail: zvi@iph.krasn.ru

Received December 21, 2006

Abstract—The paper reports on the results of ab initio calculations of the static and dynamic properties of the $LaMnO_3$ crystal with a perovskite structure in the cubic, rhombohedral, and orthorhombic phases. The calculations are performed within the ionic crystal model, which takes into account the deformability and polarizability of the ions. It is revealed that the spectrum of lattice vibrations in the cubic phase contains unstable vibrational modes, which occupy the phase space in the entire Brillouin zone. The eigenvectors of the softest mode at the boundary point *R* of the Brillouin zone are associated with the displacements of the oxygen ions and correspond to the "rotation" of the MnO_6 octahedron. The condensation of one, two, and three components of this mode leads to the tetragonal, orthorhombic, and rhombohedral distortions of the structure. The structural phase transition is described in terms of the local mode approximation with the use of the double perovskite unit cell, in which the MnO_6 octahedron is explicitly separated. The parameters of the model Hamiltonian are determined. The static properties are investigated by the Monte Carlo method. The calculated temperature of the phase transition from the cubic phase (9800 K) is considerably higher than the melting temperature of the crystal under investigation. The calculated frequencies of long-wavelength lattice vibrations in the experimentally observed orthorhombic and rhombohedral phases are in reasonable agreement with experimental data.

PACS numbers: 63.20.Dj, 64.60.-i, 64.70.Kb

DOI: 10.1134/S1063783407090235

1. INTRODUCTION

Manganites with the general formula $R_{1-x}A_xMnO_3$ (*R* is a rare-earth element; *A* = Ca, Sr, Ba, or Pb) and a perovskite structure possess interesting physical properties and have been investigated for several decades.

The phase diagrams and physical properties of solid solutions based on some compounds can change radically with a variation in the concentration of solution components [1–6]. For example, the $La_{1-x}Ca_xMnO_3$ solid solutions undergo a metal–insulator phase transition at concentrations $0.20 \le x \le 0.48$ and remain insulators at other concentrations [7]. Moreover, individual compounds and their solid solutions can undergo various structural phase transitions depending on the composition, and the physical properties of materials depend substantially on distortions of the crystal lattice [8–12]. A hypothesis has been proposed that lattice crystal vibrations make a significant contribution to unusual properties of manganites. Therefore, information on the phonon spectrum of these compounds is important for the understanding of their properties.

The crystal structure of the main representative $LaMnO_3$ of this group of compounds depends on the synthesis conditions. The $LaMnO_3$ manganite of the stoichiometric composition crystallizes in an orthorhombic structure (space group *Pnma*) with four molecules ($Z = 4$) in the unit cell [8, 9]. This orthorhombic structure is a distorted modification of the perfect perovskite structure, in which the distortions are predominantly associated with the oxygen ion displacements resulting in "rotations" of MnO_6 octahedra. The rhombohedral phase of the $LaMnO_3$ crystal with space group $R\bar{3}c$ ($Z = 2$) was observed in different works at temperatures above 300 [9, 13] and 800 K [10]. The rhombohedral structure is also a distorted modification of the perfect perovskite structure, in which the distortions are due to the rotations of MnO_6 octahedra. The cubic phase of the $LaMnO_3$ crystal was observed at temperatures above 1200 K only by Rudskaya et al. [10]. According to the results of other structural investigations, no cubic phase with a perovskite structure is observed up to the melting temperature [11]. The phonon spectra of the $LaMnO_3$ manganite have been studied in the orthorhombic and rhombohedral phases.

The IR- and Raman-active phonons in the orthorhombic phase of the $LaMnO_3$ manganite were investigated by Iliev et al. [14] and Fedorov et al. [15]. These authors also calculated the limiting frequencies of lattice vibrations in terms of the shell model with empiri-

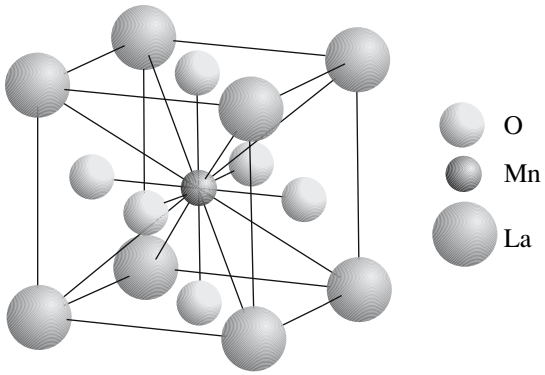

Fig. 1. Crystal structure of the $LaMnO_3$ compound in the cubic phase with symmetry space group $Pm\bar{3}m$.

cal fitting parameters. The measured vibrational frequencies and the results of similar calculations for the rhombohedral phase of the $LaMnO_3$ crystals are given in [13]. Nikiforov and Popov [16] calculated the phonon spectrum of the $LaMnO_3$ compound in the framework of the shell model and with allowance made for the Jahn–Teller contribution to the dynamic matrix for the perfect perovskite structure and obtained imaginary frequencies of vibrations in the vicinity of the symmetry points R and M in the Brillouin zone.

The purpose of this study was to calculate the overall spectrum of lattice vibrations and the rf permittivities of the $LaMnO_3$ crystal in the unstable cubic and tetragonal phases, as well as in the stable orthorhombic and rhombohedral phases, within the ab initio approach in terms of the ionic crystal model with polarizable ions of equilibrium volume. Moreover, the instability temperature of the cubic phase was calculated by the effective Hamiltonian method in the local mode approximation.

Section 2 of this paper presents the results of calculations of the frequencies of normal lattice vibrations, Born dynamic charges, elastic moduli, and rf permittivities of the $LaMnO_3$ crystal with a perfect perovskite structure.

The parameters of the effective Hamiltonian, which describes the structural phase transition associated with the instability of the cubic phase with respect to the vibrational mode whose eigenvector corresponds to the rotation of the MnO_6 octahedron, are determined in Section 3. The phase transition temperatures and the temperature dependences of the order parameter and the heat capacity are calculated by the Monte Carlo method.

The vibrational frequencies, elastic moduli, and permittivities for the rhombohedral and orthorhombic phases of the $LaMnO_3$ crystal are calculated and compared with the available experimental data and results of other calculations in Section 4.

2. LATTICE DYNAMICS OF THE $LaMnO_3$ MANGANITE IN THE CUBIC PHASE

The equilibrium volume, vibrational frequencies, Born dynamic charges, elastic moduli, and rf permittivities were calculated within the ionic crystal model, which takes into account the deformability and the dipole and quadrupole polarizabilities of the ions [17, 18]. The model and the calculation procedure are described in detail in the review [19] and in our earlier works [20, 21].

The crystal structure of the $LaMnO_3$ manganite in the cubic phase with space group $Pm\bar{3}m$ is shown in Fig. 1. The equilibrium value of the lattice parameter a_0

Table 1. Dynamic ionic charges and permittivities of the $LaMnO_3$ crystal in the cubic, rhombohedral, and orthorhombic phases

Cubic phase		Rhombohedral phase (in the rectangular coordinate system)				Orthorhombic phase			
atom	Z^{din}	atom	Z^{din}_{xx}	Z^{din}_{yy}	Z^{din}_{zz}	atom	Z^{din}_{xx}	Z^{din}_{yy}	Z^{din}_{zz}
La	3.92	La	3.63	4.05	4.05	La	3.86	3.78	4.13
Mn	3.48	Mn	3.22	3.32	3.51	Mn	3.33	3.46	3.52
$O_{\parallel}$	–2.73	O	–2.76	–2.41	–2.10	O1	–2.23	–2.70	–2.54
$O_{\perp}$	–2.33					O2	–2.48	–2.27	–2.56
ε_∞	3.21		$\varepsilon^{xx}_\infty = 2.90$	$\varepsilon^{yy}_\infty = 3.09$	$\varepsilon^{zz}_\infty = 3.09$		$\varepsilon^{xx}_\infty = 3.03$	$\varepsilon^{yy}_\infty = 3.04$	$\varepsilon^{zz}_\infty = 3.00$

was determined from the minimum in the dependence of the total energy of the crystal on the volume and amounted to 3.87 Å. The calculated rf permittivities and dynamic ionic charges of the crystal under investigation are listed in Table 1. The calculated elastic moduli are given in Table 2. It should be noted that the dynamic ionic charges in the $LaMnO_3$ crystal differ from those in oxygen-containing ferroelectrics with a perovskite structure. In the latter compounds, the charge of the cation located at the center of the octahedron and the component of the dynamic charge of oxygen along the B–O bond considerably exceed the nominal ionic charge, whereas the corresponding excess in the manganite under consideration is insignificant.

The calculated dispersion curves for the frequencies of lattice vibrations in the $LaMnO_3$ crystal in the cubic phase are depicted in Fig. 2. It can be seen from this figure that the spectrum of lattice vibrations contains the imaginary frequencies. This indicates that the cubic phase of the manganite is structurally unstable. It should be emphasized that the unstable modes occupy the whole phase space in the Brillouin zone and the absolute values of the softest modes at the symmetry points R (the R_{25} mode) and M (the M_3 mode) in the Brillouin zone are comparable in magnitude. The calculated spectrum of lattice vibrations in the cubic phase differs from the phonon spectrum obtained in [16], which, as was noted above, contains the unstable modes only in the vicinity of the symmetry points R and M. The triply degenerate mode R_{25} has eigenvectors that correspond only to displacements of the oxygen atoms; that is,

$$O1y = -O2z,$$
$$O1x = -O3z,$$
$$O2x = -O3y.$$

The nondegenerate mode M_3 also corresponds only to displacements of the oxygen atoms; that is,

$$O2x = -O3y.$$

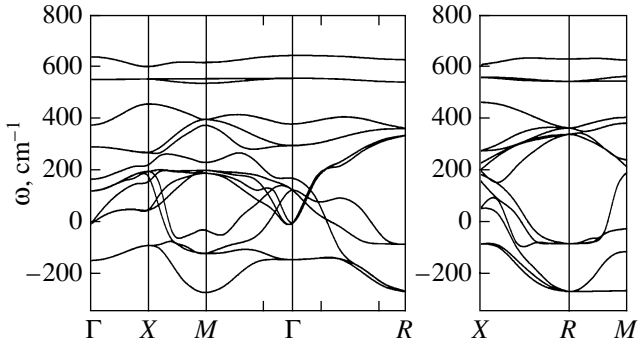

Fig. 2. Phonon spectrum of the $LaMnO_3$ crystal in the cubic phase. The negative values correspond to the imaginary frequencies.

Table 2. Elastic moduli (10^{12} dyn/cm^2) of the $LaMnO_3$ crystal in the cubic and orthorhombic phases

Cubic phase (calculation performed in this work)		Orthorhombic phase (calculation performed in this work)		Orthorhombic phase (the experimental data taken from [22])	
C_{11}	2.80	C_{11}	2.45	C_{11}	3.05
C_{12}	0.80	C_{22}	2.60	C_{12}	1.08
C_{44}	0.82	C_{33}	3.12		
		C_{12}	1.03		
		C_{13}	0.87		
		C_{23}	1.01		
		C_{44}	0.99		
		C_{55}	0.84		
		C_{66}	1.00		

3. STRUCTURAL PHASE TRANSITIONS

As was noted above, the softest modes in the structure of the $LaMnO_3$ crystal are the R_{25} and M_3 modes, which belong to the boundary points of the Brillouin zone. The phase transition associated with the condensation of these modes is accompanied by an increase in the unit cell volume. In the perovskite structure, the BO_6 octahedra are shared by vertices. In order to separate explicitly the MnO_6 octahedron, we consider the compound with the double chemical formula $La_2Mn_2O_6$ (Fig. 3) with space group $Fm\bar{3}m$ and one molecule in the unit cell (the elpasolite structure). Two manganese ions formally differ from each other in that the distances between the manganese and oxygen ions

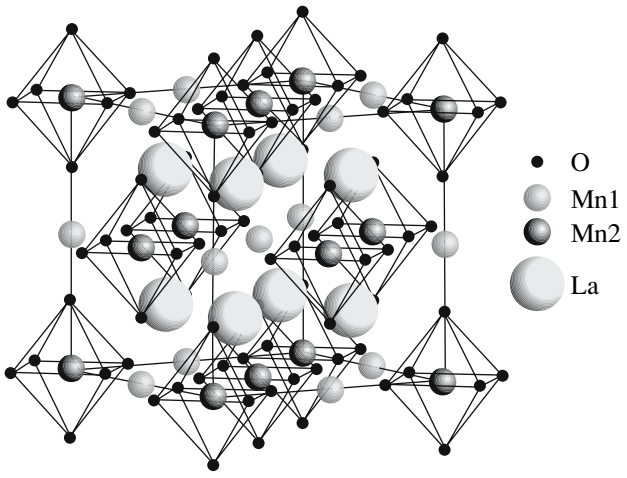

Fig. 3. Crystal structure with the double chemical formula $La_2Mn_2O_6$ and symmetry space group $Fm\bar{3}m$ (the elpasolite structure).

Table 3. Eigenvectors of the triply degenerate vibrational mode T_{1g}

ξ_i	La1	La2	O1	O2	O3	O4	O5	O6	Mn1	Mn2
ξ_x	000	000	$0\frac{1}{2}0$	$0-\frac{1}{2}0$	$00\frac{1}{2}$	$00-\frac{1}{2}$	000	000	000	000
ξ_y	000	000	$\frac{1}{2}00$	$-\frac{1}{2}00$	000	000	$00-\frac{1}{2}$	$00\frac{1}{2}$	000	000
ξ_z	000	000	000	000	$-\frac{1}{2}00$	$\frac{1}{2}00$	$0\frac{1}{2}0$	$0-\frac{1}{2}0$	000	000

differ by an arbitrarily small quantity Δ: Mn1–O = $a_0/2(1 - \Delta)$ and Mn2–O = $a_0/2(1 + \Delta)$, where a_0 is the lattice parameter of the perovskite structure. In this case, point symmetry is conserved and only translational symmetry of the perovskite structure is lost. For the given double unit cell, the center and the boundary point R of the Brillouin zone of the simple cubic lattice of the perovskite structure change over into the center of the Brillouin zone of the face-centered lattice and the boundary points M and X of the simple lattice change over into the boundary point of the face-centered lattice. The triply degenerate mode R_{25} at the boundary point R of the perovskite structure becomes the triply degenerate mode T_{1g} at the center of the Brillouin zone with the following eigenvectors:

$$-O1y = O2y = O5z = -O6z,$$
$$-O1x = O2x = -O3z = -O4z,$$
$$-O3y = O4y = -O5x = O6x.$$

These displacements of the oxygen ions correspond to the rotation of the $Mn1O_6$ octahedron. The phase transition to the tetragonal phase is associated with the condensation of one of the components of the triply degenerate mode T_{1g} at the center of the Brillouin zone. The condensation of the soft mode at the X point also leads to a tetragonal structural distortion, but with the doubling of the unit cell volume of the face-centered cubic lattice. For Δ = 0, it is possible to choose the body-centered tetragonal unit cell with two molecules.

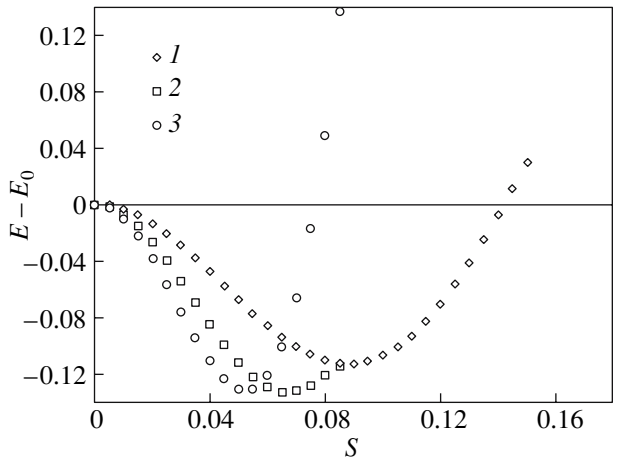

Fig. 4. Dependences of the total energy of the crystal on (*1*) one, (*2*) two, and (*3*) three components of the uniform displacements in the local mode.

In order to describe the phase transition associated with the condensation of the T_{1g} (or X_3) mode, we use the local mode approximation in which only the degrees of freedom associated with this mode are taken into account. The local mode has the form

$$S_\alpha = \frac{1}{a_0}\sum_k \xi_{\alpha k} v_k^{\mathrm{O}},$$

where v_k^{O} is the amplitude of displacements of the oxygen ions and ξ_k is the eigenvector of the T_{1g} mode (Table 3).

The microscopic model Hamiltonian that describes the system of three-component local modes (pseudovectors) located at sites of the face-centered cubic lattice includes the anharmonic terms of the one-site potential and pair interactions between local modes at different lattice sites; that is,

$$H = \sum_i (H_i^{\mathrm{anh}} + H_i^{\mathrm{ss}}),$$

$$H_i^{\mathrm{anh}} = A\{S_{i\alpha}^2\} + B\{S_{i\alpha}^4\} + C\{S_{i\alpha}^2 S_{i\beta}^2\}, \qquad (1)$$

$$H_i^{\mathrm{ss}} = a_k\{S(\mathbf{r})S(\mathbf{r}')\} + b_k\{S(\mathbf{r})S(\mathbf{r}')\},$$

where the constants a_1, a_2, and a_3 describe the interactions in the first coordination sphere and the constants b_1 and b_2 describe the interactions between the second neighbors. The explicit form of the Hamiltonian H_i^{ss} with due regard for the transformation properties of the local mode and for the lattice symmetry is given in our previous work [21]. The parameters of Hamiltonian (1) were determined by calculating the total energy of the low-symmetry phases with uniform and nonuniform distortions from the eigenvectors of the local mode. The

parameters of the one-site anharmonic potential were found from the dependences of the total energy of the crystal on the amplitude of one, two, and three components of the uniform displacements in the local mode. These dependences are plotted in Fig. 4. The parameters of the pair interactions were obtained from the differences between the total energies of the undistorted and distorted phases at the amplitude $S/2a_0 = 0.09$:

$$\begin{cases} 4a_1 + 8a_2 + 2b_1 + 4b_2 + A = E_1 - E_0 = -3.07\ (\text{eV}) \\ 4a_1 - 8a_2 + 2b_1 + 4b_2 + A = E_2 - E_0 = -3.22\ (\text{eV}) \\ 4a_1 - 2b_1 + 4b_2 + A = E_3 - E_0 = -1.86\ (\text{eV}) \\ -24a_3 - 6b_1 - 12b_2 + 3A = E_4 - E_0 = -0.35\ (\text{eV}) \\ -4a_1 + 2b_1 + 4b_2 + A = E_5 - E_0 = 4.27\ (\text{eV}) \\ +2b_1 + 4b_2 + A = E_6 - E_0 = 0.57\ (\text{eV}). \end{cases} \quad (2)$$

Here, E_0 is the energy of the undistorted cubic phase; E_1 is the energy of the phase with the distortions associated with the condensation of one component of the local mode at the center of the Brillouin mode of the face-centered cubic lattice; E_2 and E_3 are the energies of the distorted phases due to the condensation of one component of the local mode at the boundary point $X = 2\pi/2a_0(1, 0, 0)$ and at the point $\Lambda = \pi/2a_0(1, 0, 0)$, respectively; E_4 is the energy of the distorted phase due to the condensation of three components of the local mode at the boundary point $L = \pi/2a_0(1, 1, 1)$ of the Brillouin zone; E_5 is the energy of the phase distorted by the rotation of the octahedron around the [100] axis with the doubling of the unit cell along the [001] axis; and E_6 is the energy of the phase with the quadruple volume of the unit cell, in which one octahedron is rotated around the [100] axis and the other three octahedra are rotated around the same axis but in the opposite direction.

The calculated parameters of the Hamiltonian are presented in Table 4. We could not construct the equation in which it would be possible to separate the parameters b_2 and A in the system of equations (2) and set $b_2 = 0.5a_1$. For smaller values of the constant b_2, the parameter A appears to be smaller than zero; i.e., the one-site anharmonic potential becomes a multiminimum potential. It is worth noting that the constant a_2 is small in magnitude. This constant is determined from the difference between the energies of the distorted phases due to the uniform and nonuniform rotations of the $Mn1O_6$ octahedron around one of the crystallographic axes of the cubic phase. The corresponding distortions are associated either with the condensation of one component of the R_{25} mode (the uniform rotation of the octahedron in the elpasolite structure) or with the condensation of the M_3 mode. The energies of these distorted phases (at $\Delta = 0$, with symmetry $I4/mcm$ and $P4/mbm$, respectively) are nearly equal to each other.

Table 4. Coefficients of the model Hamiltonian (given in electron-volts)

One-site coefficients	
A	21.29
B	2.30×10^3
C	5.36×10^3
Interstitial coefficients	
a_1	–28.82
a_2	0.29
a_3	15.42
b_1	–9.88
b_2	–14.41

The statistical properties of the system with the model Hamiltonian (1) under consideration were investigated by the Monte Carlo method. The calculations were performed using the conventional Monte Carlo algorithm [23]. We examined crystal lattices $10 \times 10 \times 10$ and $20 \times 20 \times 20$ in size with periodic boundary conditions. The Monte Carlo procedure was started at both high and low temperatures with different initial configurations (the completely disordered configuration with $S = 0$ at all lattice sites and the completely ordered configurations with $S_x = 0.09 \times 2a_0$, $S_y = S_z = 0$, and $S_x = S_y = S_z = 0.052 \times 2a_0$). The phase transition temperature was estimated from the peak in the temperature dependence of the heat capacity. When starting at high temperatures irrespective of the initial configuration, the system undergoes a second-order phase transition at a temper-

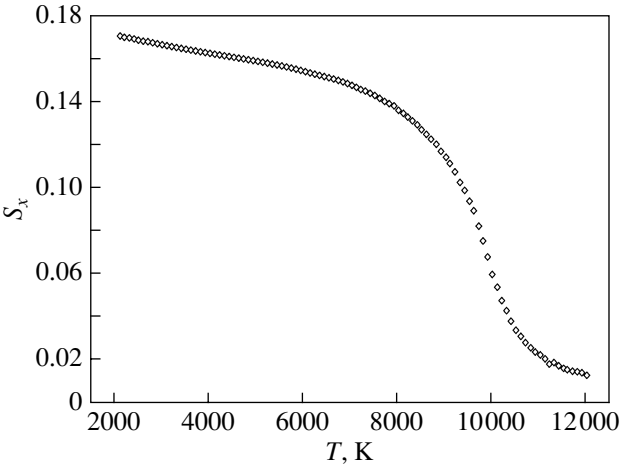

Fig. 5. Temperature dependence of the order parameter according to the Monte Carlo calculations (when the Monte Carlo procedure started at low temperatures with the initial configuration $S_x = 0.09 \times 2a_0$ and $S_y = S_z = 0$).

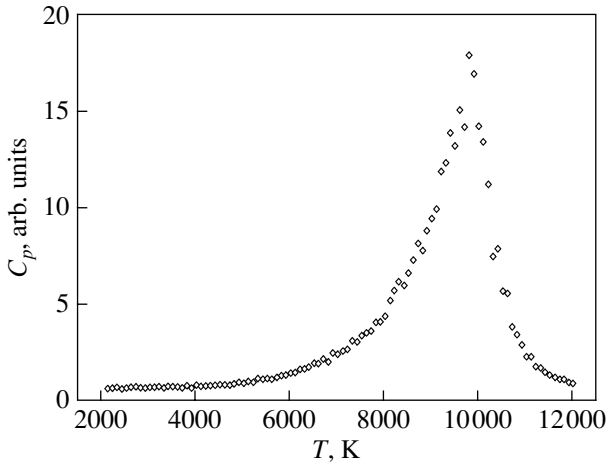

Fig. 6. Temperature dependence of the heat capacity according to the Monte Carlo calculations.

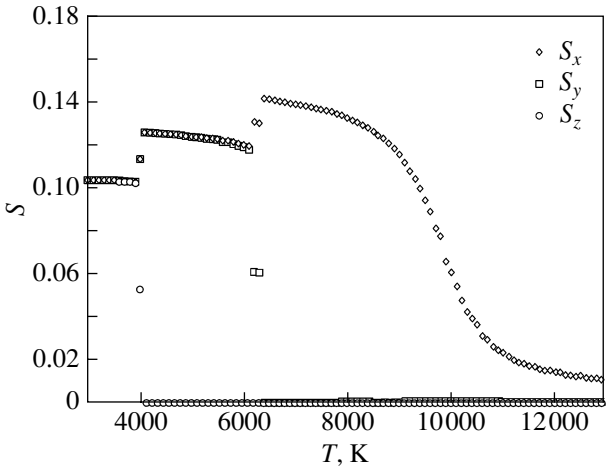

Fig. 7. Temperature dependence of the order parameter according to the Monte Carlo calculations (when the Monte Carlo procedure started at low temperatures with the initial configuration $S_x = S_y = S_z = 0.052 \times 2a_0$).

ature of 9800 K to the tetragonal phase with one nonzero component of the order parameter and this phase is retained at all temperatures below the transition temperature. When starting at low temperatures, the behavior of the system depends on the initial configuration specified at the first step of the procedure. For the initial configuration with $S_x = 0.09 \times 2a_0$ and $S_y = S_z = 0$, it can be seen from the temperature dependences of the order parameter (Fig. 5) and the heat capacity (Fig. 6) that the system undergoes one second-order phase transition from the completely ordered tetragonal phase to the completely disordered phase at a temperature of 9800 K. In the case of the initial configuration with $S_x = S_y = S_z = 0.052 \times 2a_0$ (the phase with orthorhombic symmetry $R\bar{3}c$ and two molecules in the unit cell), it can be seen from Fig. 7 that the system is characterized by the sequence of two first-order phase transitions, namely, rhombohedral phase ($\langle S_x\rangle = \langle S_y\rangle = \langle S_z\rangle \neq 0$) $\longrightarrow$ (4000 K) orthorhombic phase ($\langle S_x\rangle = \langle S_y\rangle \neq 0$, $\langle S_z\rangle = 0$, symmetry *Imam* with two molecules in the unit cell) $\longrightarrow$ (6100 K)

Table 5. Vibrational frequencies ω_i at $q = 0$ in the crystal lattice of the $LaMnO_3$ crystal in the tetragonal phase

Symmetry	ω_i, cm^{-1}	
	the amplitude of the displacement of oxygen ions is 0.05	the amplitude of the displacement of oxygen ions is 0.09
A_{1g}	117	345
A_{2g}	498	216
	588	558
B_{1g}	481	364
B_{2g}	34	119
	347	367
E_g	26*i*	120
	222*i*	122
	355	334
A_{1u}	360	360
A_{2u}	192	216
	392	414
	635	629
B_{1u}	225	346
E_u	101*i*	60
	182	224
	292	255
	334	286
	486	381

Table 6. Unit cell parameters and fractional coordinates of atoms in the structure of the $LaMnO_3$ crystal in the rhombohedral phase (space group $R\bar{3}c$, hexagonal setting) (the experimental data taken from [9] are given in parentheses)

Unit cell parameters, Å		*a*	*b*	*c*
		5.4687 (5.5285)	5.4687 (5.5285)	13.3956 (13.3348)
Atom	Wyckoff position	*x*	*y*	*z*
La	6*a*	0.0000 (0.0000)	0.0000 (0.0000)	0.2500 (0.2500)
Mn	6*d*	0.0000 (0.0000)	0.0000 (0.0000)	0.0000 (0.0000)
O	18*e*	0.4200 (0.4466)	0.0000 (0.0000)	0.2500 (0.0000)

Table 7. Vibrational frequencies ω_i (cm^{-1}) at $q = 0$ in the crystal lattice of the $LaMnO_3$ crystal in the rhombohedral phase

Symmetry	Lattice dynamics calculations [13]	Raman spectra [13]	IR spectra [13]	Calculation performed in this work
A_{1g}	249	236		222
A_{2g}	139			47*i*
	441			332
	716			582
E_g	42	179		117*i*
	163	520		115
	468	640		337
	646			457
A_{1u}	320			305
	361			327
A_{2u}	162/216		152/192	86*i*/168
(*TO*/*LO*)	310/465		315/441	299/372
	641/645		586/655	468/576
E_u	180/213			50/165
(*TO*/*LO*)	240/241			184/210
	317/326			297/326
	357/488			330/398
	642/645			474/589

Table 8. Unit cell parameters and fractional coordinates of atoms in the structure of the $LaMnO_3$ crystal in the orthorhombic phase (space group *Pnma*) (the experimental data taken from [8] are given in parentheses)

Unit cell parameters, Å		*a*	*b*	*c*
		5.422 (5.742)	7.670 (7.668)	5.422 (5.532)
Atom	Wyckoff position	*x*	*y*	*z*
La	4*c*	0.550 (0.549)	1/4 (1/4)	0.020 (0.010)
Mn	4*a*	0	0	0
O1	4*c*	0.000 (–0.014)	1/4 (1/4)	–0.100 (–0.070)
O2	8*d*	0.320 (0.309)	0.050 (0.039)	0.220 (0.224)

tetragonal phase ($\langle S_x \rangle \neq 0$, $\langle S_y \rangle = \langle S_z \rangle = 0$, symmetry *I*4/*mcm*), and the second-order phase transition at a temperature of 9800 K from the tetragonal phase to the cubic phase ($\langle S_x \rangle = \langle S_y \rangle = \langle S_z \rangle = 0$). It should be emphasized that all the phase transition temperatures obtained from these calculations are substantially higher than the melting temperature and, hence, the orthorhombic (*Imam*), tetragonal, and cubic phases are praphases for the experimentally observed orthorhombic phase with space group *Pnma* and four molecules in the unit cell.

4. LATTICE DYNAMICS OF DISTORTED PHASES OF THE $LaMnO_3$ MANGANITE

4.1. The Tetragonal Phase

Let us consider the tetragonal phase associated with the distortion of the perfect perovskite structure upon condensation of one component of the R_{25} (T_{1g}) mode. The unit cell in space group *I*4/*m* (*I*4/*mcm* at $\Delta = 0$) contains two $LaMnO_3$ molecules. The calculated frequencies of lattice vibrations in the tetragonal phase with the amplitudes of the displacement of oxygen ions $S/2a_0 = 0.09$ and 0.05 at $q = 0$ and $2\pi/2a_0(001)$ are listed in Table 5. As can be seen from this table, the tetragonal phase of the $LaMnO_3$ manganite is also unstable. Apart from the oxygen ions, the lanthanum ions are also displaced in the eigenvectors of the soft modes. It should be noted that, at the maximum displacements of the oxygen ions, the tetragonal phase becomes stable with respect to the vibrational modes at the boundary points of the Brillouin zone. However, when the order parameter *S* does not reach saturation, the lattice instability is retained with respect to the vibrational mode at the *Z* point of the Brillouin zone of the tetragonal structure. The tetragonal phase in the $LaMnO_3$ manganite is not observed experimentally.

4.2. The Rhombohedral Phase

The rhombohedral phase is associated with the distortion of the perovskite structure upon condensation of three components of the R_{25} (T_{1g}) mode. The unit cell in space group $R\bar{3}c$ contains two $LaMnO_3$ molecules. In the crystal under consideration, this phase is experimentally observed at high temperatures (the temperature of the transition from the orthorhombic phase to the rhombohedral phase according to different experimental data lies in the large range 300–800 K [9, 10, 13]). The calculated unit cell parameters and the atomic coordinates in the rhombohedral phase together with the experimental data are presented in Table 6. It can be seen from this table that the calculated and experimental lattice parameters coincide accurate to within 1% and that the calculated coordinates of the oxygen ions differ by 5% from the experimental values [9]. The calculated values of the Born dynamic charges and rf permittivities of the $LaMnO_3$ crystal in the rhombohedral phase are given in Table 1, and the vibrational frequencies at $q = 0$ together with the experimental data are presented in Table 7. The vibrational frequencies calculated in terms of the shell

Table 9. Vibrational frequencies ω_i (cm^{-1}) at $q = 0$ in the crystal lattice of the $LaMnO_3$ crystal in the orthorhombic phase

Symmetry	Lattice dynamics calculations [14]	Experimental Raman spectra [14]	Calculation performed in this work	Symmetry	Lattice dynamics calculations [15]	Experimental IR spectra [15	Calculation performed in this work
A_g	81		32	A_u			67
A_g	162		65	A_u			113
A_g	246	140	160	A_u			218
A_g	263	198	202	A_u			229
A_g	326	257	268	A_u			290
A_g	480	284	347	A_u			332
A_g	582	493	456	A_u			432
				A_u			485
B_{1g}	182		117	B_{1u}	76		41
B_{1g}	254	184	168	B_{1u}	194	194	183
B_{1g}	347		295	B_{1u}	273		209
B_{1g}	575		449	B_{1u}	318		253
B_{1g}	693		541	B_{1u}	334		308
				B_{1u}	419		347
				B_{1u}	431	438	375
				B_{1u}	495	469	423
				B_{1u}	577	574	603
B_{2g}	123		93	B_{2u}	191		42
B_{2g}	150		97	B_{2u}	233		166
B_{2g}	218	109	133	B_{2u}	283		287
B_{2g}	369	170	284	B_{2u}	388	247	276
B_{2g}	464	308	338	B_{2u}	412	368	321
B_{2g}	509	481	429	B_{2u}	580	416	442
B_{2g}	669	611	551	B_{2u}	625	621	483
B_{3g}	158		73	B_{3u}	117		61
B_{3g}	343		263	B_{3u}	233		97
B_{3g}	462	320	367	B_{3u}	276		193
B_{3g}	603		441	B_{3u}	294	287	234
B_{3g}	692		555	B_{3u}	332	344	241
				B_{3u}	401	384	288
				B_{3u}	443	455	380
				B_{3u}	521	510	437
				B_{3u}	580	594	507

model of the ionic crystal with empirical fitting parameters are also listed in Table 7. It can be seen from this table that the results of our calculations are in reasonable agreement with both the experimental data and the results of empirical calculations [13]. The maximum difference between the vibrational frequencies is approximately equal to 30%. However, according to our calculations, the rhombohedral phase turns out to be also unstable with respect to nonpolar vibrations of the crystal lattice.

4.3. The Orthorhombic Phase

The orthorhombic phase with space group D_{2h}^{16} and four molecules in the unit cell is associated with the uniform distortion of the elpasolite unit cell due to the condensation of two components of the T_{1g} mode (the R_{25} mode in the perovskite structure) and with the nonuniform distortion of this unit cell as a result of the condensation of the X_3 mode at the boundary point of the Brillouin zone of the elpasolite structure (or, what is the same, the M_3 mode in the perfect perovskite structure). However, it follows from our calculations that, when only displacements of the oxygen ions in the orthorhombic phase are taken into account, the spectrum of lattice vibrations involves imaginary frequencies of vibrations. Since the orthorhombic phase is formed upon the sequential (at least) two phase transitions from the cubic phase to the tetragonal phase and then to the orthorhombic phase, we obtained the orthorhombic phase due to the ionic displacements according to the eigenvector of the unstable vibrational mode of the tetragonal phase, when, apart from the oxygen ions, the lanthanum atoms are involved in the displacement. The displacements were chosen so that the spectrum of lattice vibration frequencies did not contain unstable modes. The calculated unit cell parameters and the atomic coordinates in the orthorhombic phase together with the experimental data taken from [8] are presented in Table 8. The calculated components of the permittivity tensors and dynamic charges are given in Table 1. The elastic moduli for the orthorhombic phase of the crystal under investigation are listed in Table 2. The calculated frequencies of lattice vibrations at $q = 0$ together with the experimental data are presented in Table 9. For comparison, this table also includes the results of the empirical calculations carried out in [14, 15]. It can be seen from Tables 2, 8, and 9 that the calculated values of the unit cell parameters, atomic coordinates, and limiting vibrational frequencies are in satisfactory agreement with the experimental data.

5. CONCLUSIONS

Thus, the atomic properties, the permittivity, and the vibrational frequencies of the $LaMnO_3$ crystal in the cubic, tetragonal, rhombohedral, and orthorhombic phases were calculated in the framework of the ab initio approach. It was revealed that the experimentally not observed cubic phase of the crystal appears to be unstable to the lattice vibrational modes that occupy the whole phase space in the Brillouin zone. The parameters of the model Hamiltonian that describes the structural transition from the cubic phase were determined within the local mode approximation. The temperature of this transition, which was calculated by the Monte Carlo method, turned out to be considerably higher than the melting temperature of the crystal under investigation. The calculated unit cell parameters, coordinates of ions, elastic moduli, and frequencies of lattice vibrations in the experimentally observed rhombohedral and orthorhombic phases are in reasonable agreement with the experimental data. The inference was made that the proposed ab initio ionic crystal model accounting for the dipole and quadrupole polarizability of the ions correctly describes the structural properties and the lattice dynamics of the $LaMnO_3$ crystal.

ACKNOWLEDGMENTS

This study was supported by the Russian Foundation for Basic Research (project no. 06-02-16091) and the Council on Grants from the President of the Russian Federation for Support of Leading Scientific Schools of the Russian Federation (grant no. NSh-4137.2006.2).

REFERENCES

1. Yu. A. Izyumov and Yu. N. Skryabin, Usp. Fiz. Nauk **171** (2), 121 (2001) [Phys. Usp. **44** (2), 119 (2001)].
2. M. Yu. Kagan and K. I. Kugel', Usp. Fiz. Nauk **171** (6), 577 (2001) [Phys. Usp. **44** (6), 553 (2001)].
3. V. M. Loktev and Yu. G. Pogorelov, Fiz. Nizk. Temp. (Kharkov) **26** (3), 231 (2000) [Low Temp. Phys. **26** (3), 171 (2000)].
4. É. L. Nagaev, Usp. Fiz. Nauk **166** (8), 833 (1996) [Phys. Usp. **39** (8), 781 (1996)].
5. M. B. Salamon and M. Jaime, Rev. Mod. Phys. **73**, 583 (2001).
6. E. O. Wollan and W. C. Koehler, Phys. Rev. **100**, 545 (1955).
7. A. J. Millis, Nature (London) **392**, 147 (1998).
8. J. B. A. A. Elemans, B. van Laar, K. R. van der Veen, and B. O. Loopstra, J. Solid State Chem. **3**, 238 (1971).
9. Q. Huang, A. Santoro, J. W. Lynn, R. W. Erwin, J. A. Borchers, J. L. Peng, and R. L. Greene, Phys. Rev. B: Condens. Matter **55**, 14987 (1997).
10. A. G. Rudskaya, N. B. Kofanova, L. E. Pustovaya, B. S. Kul'buzhev, and M. F. Kupriyanov, Fiz. Tverd. Tela (St. Petersburg) **46** (10), 1856 (2004) [Phys. Solid State **46** (10), 1922 (2004)].
11. J. Rodriguez-Carvajal, M. Hennion, F. Moussa, and A. H. Moudden, Phys. Rev. B: Condens. Matter **57**, R3189 (1998).
12. V. S. Gaviko, A. V. Korolev, V. E. Arkhipov, N. G. Bebenin, and Ya. M. Mukovskiĭ, Fiz. Tverd. Tela (St. Petersburg) **47** (7), 1255 (2005) [Phys. Solid State **47** (7), 1299 (2005)].
13. M. V. Abrashev, A. P. Litvinchuk, M. N. Iliev, R. L. Meng, V. N. Popov, and V. G. Ivanov, Phys. Rev. B: Condens. Matter **59**, 4146 (1999).
14. M. N. Iliev, M. V. Abrashev, H.-G. Lee, V. N. Popov, Y. Y. Sun, C. Thomsen, R. L. Meng, and C. W. Chu, Phys. Rev. B: Condens. Matter **57**, 2872 (1998).

15. I. Fedorov, J. Lorenzana, P. Dore, G. de Marzi, P. Maselli, P. Calvani, S.-W. Cheong, S. Koval, and R. Migoni, Phys. Rev. B: Condens. Matter **60**, 11875 (1999).
16. A. E. Nikiforov and S. E. Popov, Fiz. Tverd. Tela (St. Petersburg) **43** (6), 1093 (2001) [Phys. Solid State **43** (6), 1132 (2001)].
17. O. V. Ivanov and E. G. Maksimov, Zh. Éksp. Teor. Fiz. **108** (5), 1841 (1995) [JETP **81** (5), 1008 (1995)].
18. O. V. Ivanov and E. G. Maksimov, Zh. Éksp. Teor. Fiz. **114** (1), 333 (1998) [JETP **87** (1), 186 (1998)].
19. E. G. Maksimov, V. I. Zinenko, and N. G. Zamkova, Usp. Fiz. Nauk **174** (11), 1145 (2004) [Phys. Usp. **47** (11), 1075 (2004)].
20. V. I. Zinenko, N. G. Zamkova, and S. N. Sofronova, Zh. Éksp. Teor. Fiz. **114** (5), 1742 (1998) [JETP **87** (5), 944 (1998)].
21. V. I. Zinenko and N. G. Zamkova, Zh. Éksp. Teor. Fiz. **118** (2), 359 (2000) [JETP **91** (2), 314 (2000)].
22. K. H. Ahn and A. J. Millis, Phys. Rev. B: Condens. Matter **64**, 115103 (2001).
23. *Monte Carlo Methods in Statistical Physics*, Ed. by K. Binder (Springer, Heidelberg, 1979; Mir, Moscow, 1982).

Translated by O. Borovik-Romanova